Simulating solid state phase transitions with the roots of transformation matrices

2009 J. Phys.: Condens. Matter 21 245404

(http://iopscience.iop.org/0953-8984/21/24/245404)

J. Phys.: Condens. Matter **21** (2009) 245404 (7pp) doi:10.1088/0953-8984/21/24/245404

Simulating solid state phase transitions with the roots of transformation matrices

O Potzel and G Taubmann

Institute of Theoretical Chemistry, University of Ulm, 89069 Ulm, Germany

E-mail: gerhard.taubmann@uni-ulm.de

Received 8 July 2008, in final form 20 April 2009
Published 26 May 2009
Online at stacks.iop.org/JPhysCM/21/245404

Abstract

We have studied the pressure induced B1–B2 phase transition within the Buerger mechanism. A transition path was generated using roots of the transition matrix between the B1 and the B2 structure. The enthalpies of activation $\Delta H^{\neq}$ were obtained for this path for the typical examples of NaCl and of CaO from first principle calculations. The results were compared to $\Delta H^{\neq}$-values for optimized transition paths either reported in the literature or obtained from our own test calculations. They were very similar to the values obtained from the matrix root method. The latter method is, however, computationally very efficient because no optimization procedure of the transition path is necessary.

This paper is dedicated to Professor Heinz-Dieter Rudolph on the occasion of his 85th birthday.

1. Introduction

For most alkaline halides and alkaline earth chalcogenides, a pressure induced phase transition from the rock-salt structure (B1) to the CsCl structure (B2) can be observed. The corresponding transition pressures range from 0.5 GPa for rubidium bromide up to about 200 GPa for magnesium oxide. Such conditions occur at various depths of the earth mantle. These phase transitions are therefore of great importance in geophysics [1] and have been investigated over a long period of time [2–4].

In most papers on this topic, the values of the transition pressure are determined using either experimental [5, 6] or theoretical methods [7–10]. The path of the transition and the corresponding energy barrier, however, have been investigated much less frequently. As long ago as 1948, Buerger [11] suggested a simple path via $R\bar{3}m$, which is a subgroup of both the space groups $Fm\bar{3}m$ of the B1 structure and $Pm\bar{3}m$ of the B2 structure. Meanwhile, all possible mechanisms of the B1–B2 transition have been investigated in great detail by Stokes and Hatch [12], who considered all subgroups common to both the initial and the final structure. According to molecular dynamics simulations [13], the Buerger mechanism is one of the most favourable transition paths.

However, usually the determination of the transition mechanism is computationally very expensive. It requires the identification of an optimized transition path involving a large number of optimization steps. Here we propose a new approximate method that is computationally much cheaper than previous methods because no relaxation along the transition path is necessary. This method is based on the nth roots of the transition matrix between initial and final structure with n being sufficiently large. The successive application of the nth root provides a reasonable guess for the transition path of relatively simple transition mechanisms, as we will show in this paper, that can then be checked by more advanced methods. For more complicated reaction mechanisms, our new method is less appropriate, but in any case it provides an upper bound for the transition barrier.

In detail, a phase transition can be described by a transformation matrix $\mathbf{T}$ connecting the matrix $\mathbf{A}$ of the primitive row vectors of the initial structure to the matrix $\mathbf{B}$ of the primitive row vectors of the target structure.

$$\mathbf{B} = \mathbf{A}\,\mathbf{T}. \tag{1}$$

Our method (MRAM: matrix root application method) uses a higher root $\mathbf{R}$ of the matrix $\mathbf{T}$. $\mathbf{A}$ is multiplied by powers of $\mathbf{R}$ in order to create intermediate structures between $\mathbf{A}$ and $\mathbf{B}$. In the calculations reported in the literature, the transition path was usually divided into ten intervals [12, 14]. Following this convention, we decided to use the tenth root $\mathbf{R} = \mathbf{T}^{1/10}$ of $\mathbf{T}$. The method works, of course, for every nth root of $\mathbf{T}$, as long as n is not too small. An example for $n \neq 10$ will be discussed at the end of section 3.

This approach using the nth root is physically motivated by the idea that the transition path connecting two structures

should be relatively simple. Using a linear geometric interpolation between initial and final structures, however, leads in general to an energetically rather costly path since typically large repulsive interactions can occur. Hence our approach can be regarded as providing the simplest reaction path connecting two structures that goes beyond the linear interpolation.

All quantum chemical calculations reported in this work were carried out using the ABINIT code [15]. ABINIT is an accurate and well documented open source density functional theory (DFT) code using a plane wave basis and periodic boundary conditions. Hartwigsen, Goedecker, Hutter pseudopotentials [16] were used in all calculations carried out in this work. The local density approximation (LDA) was used for most calculations unless otherwise indicated. Both the cutoff energy and the number of k-points were chosen large enough to allow convergence to be achieved. All quantum chemical calculations refer to the electronic ground state. No lattice vibrations were taken into account.

2. Calculation of the tenth root of T

The transformation matrix $\mathbf{T}$ from the CsCl structure ($Pm\bar{3}m$) to the rock-salt structure ($Fm\bar{3}m$) in the subgroup $R\bar{3}m$ is given by [17]

$$\mathbf{T} = \begin{pmatrix} 0 & \frac{1}{2} & \frac{1}{2} \\ \frac{1}{2} & 0 & \frac{1}{2} \\ \frac{1}{2} & \frac{1}{2} & 0 \end{pmatrix}. \tag{2}$$

Three different methods for the calculation of roots of a matrix will be given below. For our application, only real-valued matrix elements are allowed because the coordinates obtained by multiplications of $\mathbf{A}$ with powers of $\mathbf{R}$ must be real valued.

In this text, we denote matrices by bold capital letters and their corresponding matrix elements by regular letters with subscripts. Let $\mathbf{M}$ be a diagonal matrix which has only positive diagonal elements $M_{ii} > 0$. Its real-valued nth root is the diagonal matrix $\mathbf{C}$ with the elements $C_{ij} = \delta_{ij} \cdot \sqrt[n]{M_{ii}}$. A matrix $\mathbf{F}$, which has only positive eigenvalues $\lambda_i > 0$ and which can be diagonalized by means of an orthogonal transformation $\mathbf{\Lambda} = \mathbf{U}^{-1}\mathbf{F}\mathbf{U}$, has the nth root $\mathbf{U}\mathbf{C}\mathbf{U}^{-1}$ ('method 1'). The matrix elements of $\mathbf{\Lambda}$ are $\lambda_{ij} = \delta_{ij} \cdot \lambda_i$ and those of $\mathbf{C}$ are $C_{ij} = \delta_{ij} \cdot \sqrt[n]{\lambda_i}$

$$\begin{aligned} \mathbf{F} &= \mathbf{U}\mathbf{\Lambda}\mathbf{U}^{-1} = \mathbf{U}\mathbf{C}^n\,\mathbf{U}^{-1} \\ &= \underbrace{(\mathbf{U}\mathbf{C}\mathbf{U}^{-1})(\mathbf{U}\mathbf{C}\mathbf{U}^{-1})\,\cdots\,(\mathbf{U}\mathbf{C}\mathbf{U}^{-1})}_{n \text{ times}}. \end{aligned} \tag{3}$$

This method cannot be applied to $\mathbf{T}$ because it has a negative eigenvalue ($\lambda_1 = 1,\ \lambda_{2,3} = -\frac{1}{2}$).

'Method 2': analogous to the definition for operators, a function $f(\mathbf{H})$ of a matrix $\mathbf{H}$ can be evaluated by substituting $\mathbf{H}$ instead of x into the Taylor expansion of $f(x)$ around $x = 0$, well known for, e.g., $\exp\{\mathbf{H}\}$. The radius of convergence of the binomial series [18]

$$(1+x)^\mu = 1 + \binom{\mu}{1} x + \binom{\mu}{2} x^2 + \cdots \quad |x| < 1, \quad \mu \in \mathbb{R} \tag{4}$$

is, however, not infinite as in the case of the exponential function, but is unity. The norm of a real-valued symmetric matrix like $\mathbf{T}$ (2) relevant for series expansions like (4) is the maximum $\max(|\lambda_i|)$ of the absolute values of the eigenvalues λ_i of $\mathbf{H}$ (spectral norm of a symmetric matrix) [19]. The series expansion of $\mathbf{T}^\mu$ reads

$$\mathbf{T}^\mu = (\mathbf{I}+\mathbf{H})^\mu = \mathbf{I} + \binom{\mu}{1}\mathbf{H} + \binom{\mu}{2}\mathbf{H}^2 + \cdots, \tag{5}$$

where the identity matrix is denoted as $\mathbf{I}$. Since the eigenvalues of $\mathbf{H} = \mathbf{T} - \mathbf{I}$ determining the convergence of the expansion (5) are $\lambda_1 = 0$ and $\lambda_{2,3} = -3/2$, the roots of $\mathbf{T}$ cannot be evaluated using (5).

The third approach ('method 3') starts from an estimate $\mathbf{R}_0$ of an approximate tenth root matrix of $\mathbf{T}$. The final tenth root matrix $\mathbf{R}$ is expected to describe a smooth transition from the initial structure to the final structure by subsequent multiplications of the matrix of the initial structure with powers of $\mathbf{R}$. We thus expect $\mathbf{R}$ to deviate to only a small extent from an identity matrix. A useful choice for $\mathbf{R}_0$ will therefore differ only slightly from $\mathbf{I}$.

The tenth power $\mathbf{K} = (\mathbf{R}_0)^{10} = \mathbf{T} + \mathbf{\Delta}$ deviates by a matrix $\mathbf{\Delta}$ from $\mathbf{T}$. The subscript indicates the number of the iteration. For clarity, this index will be omitted for all other matrices and every individual matrix element.

Partial derivatives of the matrix elements of $(\mathbf{T}+\mathbf{\Delta})$ with respect to the matrix elements of $\mathbf{R}_0$ are evaluated numerically. In one step, only a single matrix element R_{kl} of $\mathbf{R}_0$ is varied slightly by an amount of r_{kl} defining a new matrix $\mathbf{R}_0^{(kl)}$. The initial $\mathbf{K} = (\mathbf{T}+\mathbf{\Delta})$ is subtracted from the tenth power $\mathbf{K}^{(kl)}$ of the new matrix $\mathbf{R}_0^{(kl)}$ yielding the derivatives of all matrix elements of $\mathbf{\Delta}$ with respect to R_{kl}. We choose

$$r_{kl} = \begin{cases} \frac{1}{100}\,R_{kl} & \text{for } |R_{kl}| > \epsilon \\ \epsilon & \text{for } |R_{kl}| \leqslant \epsilon \end{cases} \tag{6}$$

with $\epsilon = 10^{-7}$ and obtain the numerical derivatives as

$$\frac{\partial(\mathbf{T}+\mathbf{\Delta})_{ij}}{\partial R_{kl}} \approx \left(\frac{\partial \Delta_{ij}}{\partial R_{kl}}\right)_{\text{num}} = \frac{1}{r_{kl}}\left(K_{ij}^{(kl)} - K_{ij}\right). \tag{7}$$

The total differential of Δ_{ij} is approximated by

$$\mathrm{d}\Delta_{ij} \approx \sum_{k=1}^{3}\sum_{l=1}^{3}\left(\frac{\partial \Delta_{ij}}{\partial R_{kl}}\right)_{\text{num}} \mathrm{d}R_{kl}. \tag{8}$$

We calculate the values of the $\mathrm{d}R_{kl}$ from the 9×9 inhomogeneous system of linear equations

$$\sum_{k=1}^{3}\sum_{l=1}^{3}\left(\frac{\partial \Delta_{ij}}{\partial R_{kl}}\right)_{\text{num}} \mathrm{d}R_{kl} = -\Delta_{ij} \qquad i,j = 1,\ldots,3 \tag{9}$$

and get a new matrix $\mathbf{R}_1$ with the matrix elements $R_{kl} + \alpha\,\mathrm{d}R_{kl}$ (remember that the subscript 0 is suppressed in R_{kl}). A damping factor $0 < \alpha < 1$ can be used to stabilize the calculation, if necessary. The next iterations are carried out starting with the new $\mathbf{R}_n$ until convergence is obtained. For a real-valued initial matrix, it is guaranteed that also the root found from 'method 3' is real valued.

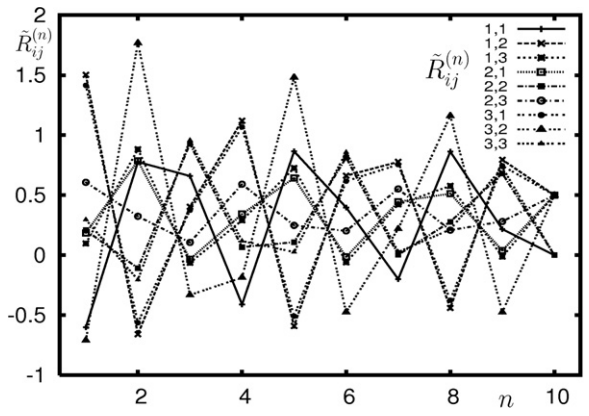

Figure 1. The matrix elements $\tilde{R}_{ij}^{(n)}$ of the powers $\tilde{\mathbf{R}}^n$ of a certain tenth root $\tilde{\mathbf{R}}$ of the transformation matrix $\mathbf{T}$. $\tilde{\mathbf{R}}$ cannot be used to describe a smooth transition from the B1 to the B2 structure as can be seen from the irregular shape of the curves.

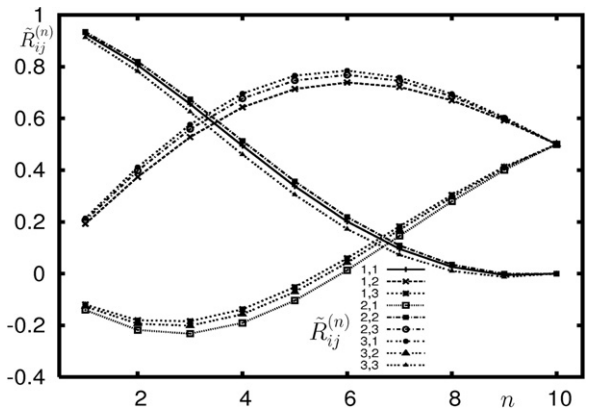

Figure 2. The matrix elements $\tilde{R}_{ij}^{(n)}$ of the powers $\tilde{\mathbf{R}}^n$ of a different tenth root $\tilde{\mathbf{R}}$ with a smooth dependence of the matrix elements on n and each three [(1, 1); (2, 2); (3, 3)], [(1, 2); (2, 3); (3, 1)], and [(1, 3); (2, 1); (3, 2)] of them having nearly the same value.

Matrices have, of course, more than one root. For the tenth roots of a given 3 × 3-matrix there are usually 10^3 different possibilities if complex-valued matrix elements are allowed. This can be easily seen considering the diagonal matrix of the eigenvalues in 'method 1'. The roots of matrices with degenerate eigenvalues not only show a discrete multiplicity but also depend on continuous parameter(s) [20]. Continuous parameters occur because the normalized eigenvectors belonging to degenerate eigenvalues are not determined uniquely.

For some choices of the initial matrix $\mathbf{R}_0$ convergence was reached within about ten iterations, whereas for other choices sometimes hundreds of thousands of iterations were necessary or no convergence was obtained at all. In the case of fast convergence, the root $\mathbf{R}$ finally obtained did not deviate much from the starting matrix $\mathbf{R}_0$ and our algorithm worked as originally intended. Here, $\mathbf{R}_n$ was a better approximation to the tenth root of $\mathbf{T}$ than $\mathbf{R}_{n-1}$. For an unfavourable choice of $\mathbf{R}_0$, however, it could happen that the coefficient matrix of the $(\partial\Delta_{ij}/\partial R_{kl})_{\mathrm{num}}$ in (9) became nearly singular in a certain step n of the iteration. The new matrix $\mathbf{R}_{n+1}$ obtained from this nth step then deviated very much from $\mathbf{R}_n$ and thus also from the initial matrix $\mathbf{R}_0$. Effectively, $\mathbf{R}_{n+1}$ acted as a new initial matrix with matrix elements completely different from those of $\mathbf{R}_0$. In the next steps, the new matrices $\mathbf{R}_{n+2}$, $\mathbf{R}_{n+3}$, ... usually improved gradually, at least as long as no other near singularity of the coefficient matrix occurred. If convergence was achieved in such a case, a root very different from $\mathbf{R}_0$ was found.

In this way, several roots were calculated. For all of them, e.g. $\tilde{\mathbf{R}}$, the individual matrix elements $(\tilde{\mathbf{R}}^n)_{ij} := \tilde{R}_{ij}^{(n)}$ of the powers $\tilde{\mathbf{R}}^n (n = 1, \ldots, 10)$ were plotted. Two typical examples are shown in figures 1 and 2. As can be seen easily from figure 2, the powers of this root interpolate smoothly between the initial and the target structure, whereas most other roots like the example shown in figure 1 are obviously useless for this purpose.

The matrix $\mathbf{T}$ has a degenerate eigenvalue. Therefore, its roots depend on a continuous parameter, as mentioned above. Each three of the matrix elements of the root shown in figure 2 have nearly the same value. The same holds for all the powers of the root. The structure of the matrices in figure 2 is very near to that of $\bar{\mathbf{R}}$ (10). The primitive vectors of the subgroup $R\bar{3}m$ all have identical lengths. Therefore, the only root $\bar{\mathbf{R}}$ suitable for the transition has to consist of only three independent matrix elements. Precise values of a, b, and c could be, in principle, obtained by playing around with a large number of slightly different matrices $\mathbf{R}_0$. Faster convergence was achieved by a modification of 'method 3', which allowed one of the nine matrix elements of $\mathbf{R}_0$ to be constrained to a fixed value.

$$\bar{\mathbf{R}} = \begin{pmatrix} a & b & c \\ c & a & b \\ b & c & a \end{pmatrix} \quad \text{with} \quad \begin{array}{l} a = 0.924\,911 \\ b = 0.204\,008 \\ c = -0.128\,919. \end{array} \tag{10}$$

Finally, the calculation was carried out constraining the structure of the root matrix to the symmetry of $\bar{\mathbf{R}}$ shown in (10). Using Maple 9.5 [21], the tenth power of $\bar{\mathbf{R}}$ was evaluated symbolically before the actual values of a, b, and c were computed numerically in a final step. It is worth mentioning that the result of a matrix multiplication of two matrices of the symmetry of $\bar{\mathbf{R}}$ is again a matrix of the same symmetry.

$$\begin{pmatrix} a & b & c \\ c & a & b \\ b & c & a \end{pmatrix} \begin{pmatrix} \alpha & \beta & \gamma \\ \gamma & \alpha & \beta \\ \beta & \gamma & \alpha \end{pmatrix} = \begin{pmatrix} A & B & C \\ C & A & B \\ B & C & A \end{pmatrix}. \tag{11}$$

Thus, the symmetry of $\bar{\mathbf{R}}$ is conserved in its powers $\bar{\mathbf{R}}^2$, $\bar{\mathbf{R}}^3$, etc. The powers of the matrix elements of $\bar{\mathbf{R}}$ look similar to those of $\tilde{\mathbf{R}}$. They are shown in figure 3. Only three curves occur, however, instead of three groups of each three adjacent curves.

3. DFT calculations of the pressure induced phase transitions

For both compounds (NaCl and CaO) in both structures (B1 and B2), we calculated about 20 energy values $E(V)$ as a function of the cell volume V. The volume range was chosen within $V \approx 0.7V_0$–$1.1V_0$, where $E_0 = E(V_0)$ denotes the

Table 1. The parameters of the fits of $E(V)$ to Birch–Murnaghan equation (12) and of the phase transition (p_{trans}, a_{B1} and a_{B2}). The expected uncertainty of p_{trans} obtained as explained in the text is given in parentheses. Due to the use of pseudopotentials, only the differences between the E_0 of the two structures of a compound are physically relevant.

Structure	E_0 (Hartree)	V_0 (Å^3)	B_0 (kbar)	B_1	Compound	p_{trans} (GPa)	a_{B1} (Å)	a_{B2} (Å)
NaCl (B1)	−62.8855	40.855	319	4.7	NaCl	27.2(3)	4.847	3.006
NaCl (B2)	−62.8753	38.378	355	4.5				
CaO (B1)	−52.9233	25.967	1300	4.3	CaO	59.5(3)	4.309	2.613
CaO (B2)	−52.8896	22.981	1380	4.2				

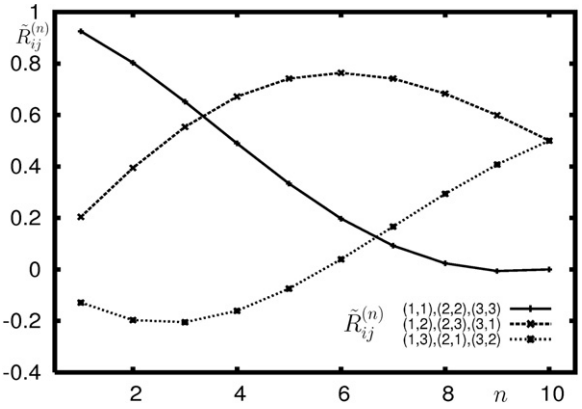

Figure 3. The matrix elements $\bar{R}_{ij}^{(n)}$ of the powers $\bar{\mathbf{R}}^n$ of the final matrix $\bar{\mathbf{R}}$ with only three independent matrix elements a, b, and c given in (10).

minimum of $E(V)$. As equation of state we used the third order Birch–Murnaghan equation $E_{\text{BM}}(V)$ [22, 23]. $B_0 = -V(\partial p/\partial V)_T$ is the bulk modulus and B_1 is its first pressure derivative, both calculated at vanishing pressure $p = 0$.

$$E_{\text{BM}}(V) = E_0 + \frac{9}{16} V_0 B_0 \left\{ \left[\left(\frac{V_0}{V} \right)^{2/3} - 1 \right]^3 B_1 + \left[\left(\frac{V_0}{V} \right)^{2/3} - 1 \right]^2 \left[6 - 4 \left(\frac{V_0}{V} \right)^{2/3} \right] \right\}. \tag{12}$$

Birch–Murnaghan functions $E_{\text{BM}}(V)$ were fitted to the energy curves $E(V)$ for each of the two structures using gnuplot 4.0 for Linux [24]. The transition pressure p_{trans} was determined by the slope of the common tangent of both $E(V)$ curves using the analytical form of $E_{\text{BM}}(V)$ (12) with the fitted parameters for both structures. We denote the points of contact as $C_{\text{B1}}(V_{\text{B1}}, E_{\text{B1}})$ and $C_{\text{B2}}(V_{\text{B2}}, E_{\text{B2}})$, respectively. The parameters of the Birch–Murnaghan curves and the transition pressures are listed in table 1.

$$p = -\left(\frac{\partial A}{\partial V} \right)_{T=0} = -\frac{\text{dE}}{\text{dV}} = -\frac{E_{\text{B2}} - E_{\text{B1}}}{V_{\text{B2}} - V_{\text{B1}}}. \tag{13}$$

Equation (13) holds because our calculations were carried out at $T = 0$ where the entropy contribution to the free energy A vanishes. The error of the transition pressure was estimated using the standard deviations (1σ) of the parameters from the fits to $E_{\text{BM}}(V)$. It can be easily seen from (13) and $H = E + pV$ that the enthalpies $H_{\text{B1}}(C_{\text{B1}})$ and $H_{\text{B2}}(C_{\text{B2}})$ at both contact points are equal.

Both the B1 and the B2 structure can be described by the matrices **A** (B1) and **B** (B2) of their primitive vectors in the common subgroup $R\bar{3}m$ [17] and the corresponding cell constants a_{B1} and a_{B2}. The latter ones were obtained from the volumes of $E_{\text{BM}}(V)$ in the two contact points with the common tangent calculated as outlined above. The numerical values of the cell constants are listed in table 1.

$$\mathbf{A} = \begin{pmatrix} 0 & \frac{1}{2} & \frac{1}{2} \\ \frac{1}{2} & 0 & \frac{1}{2} \\ \frac{1}{2} & \frac{1}{2} & 0 \end{pmatrix} \qquad \mathbf{B} = \begin{pmatrix} 1 & 0 & 0 \\ 0 & 1 & 0 \\ 0 & 0 & 1 \end{pmatrix}. \tag{14}$$

The transition path is described by the sequence

$$\mathbf{C}_n = a_{\text{B1}} c^n \mathbf{B} \bar{\mathbf{R}}^{10-n} \quad (n = 0, 1, 2, \ldots, 10) \qquad c = \sqrt[10]{\frac{a_{\text{B2}}}{a_{\text{B1}}}} \tag{15}$$

where $n = 0$ corresponds to the B1 structure and $n = 10$ to the B2 structure. The reduced coordinates are constrained to (0, 0, 0) for the metal cation and to $(\frac{1}{2}, \frac{1}{2}, \frac{1}{2})$ for the anion.

For every structure along the transition path, the energy $\bar{E}_n (n = 0, 1, 2, \ldots, 10)$ was computed. The corresponding enthalpies were calculated from $\Delta H_n = \Delta E_n + p_{\text{trans}} \cdot \Delta V_n$, where $\Delta E_n = \bar{E}_n - \bar{E}_0$ and $\Delta V_n = \bar{V}_n - \bar{V}_0$. At p_{trans}, as mentioned above, both the initial state (B1) and the final state (B2) have the same enthalpy. Thus we are free to choose either B1 or B2 as reference state. We use the B1 state and denote E_{B1} as $\bar{E}_0$ and V_{B1} as $\bar{V}_0$. The bars over the symbols are used in order to avoid confusion with the symbols in the Birch–Murnaghan equation (12). The ΔH_n-values calculated in this way for NaCl and CaO are shown in figures 4 and 5, respectively.

The enthalpy profiles of the transitions obtained from MRAM (ΔH_n) are very similar to those reported in the literature for an optimized transition path (ΔH_{rel}) [17, 25]. The reference data (ΔH_{rel}) [17, 25] were obtained from a DFT calculation using the generalized gradient approximation (GGA) functional of Perdew, Burke and Ernzerhof (PBE) [26] with the CRYSTAL98 code [27]. In order to test for the influence of different functionals, we also recalculated the enthalpies along our paths using a GGA–PBE Hamiltonian. The profiles obtained in this way were even slightly lower in enthalpy than those from LDA.

It should be stressed that the MRAM transition path based on (15) always remains within the subgroup $R\bar{3}m$. The same holds for Catti's reference values [17, 25]. Thus, the best which can be achieved with MRAM (and also with Catti's ΔH_{rel}) is the optimum path of the Buerger mechanism (i.e. via $R\bar{3}m$).

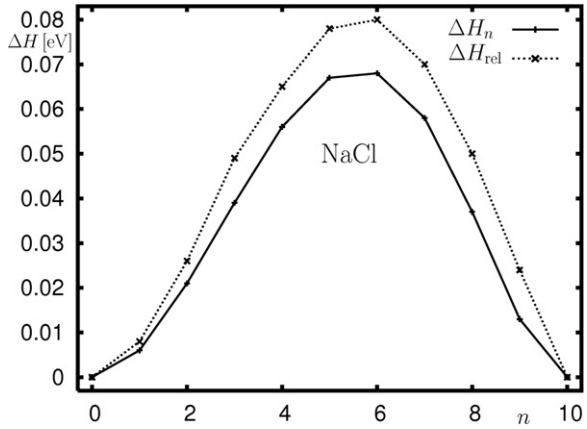

Figure 4. The enthalpy profiles of the B1–B2 transition of NaCl calculated either from the MRAM method (ΔH_n, using LDA, this work) or for a structure optimized path ($\Delta H_{\rm rel}$) reported by Catti [25]. For ΔH_n, the power of the matrix $\bar{\mathbf{R}}^n$ is denoted by n. In the case of $\Delta H_{\rm rel}$, the optimization is carried out at a constrained rhombohedral angle α with $n = 10(\alpha - \alpha_{\rm B1})/(\alpha_{\rm B2} - \alpha_{\rm B1})$ [25]. No attempt was made to obtain a smooth interpolation curve between the individual data points. The maximum of the optimized transition path ($\Delta H_{\rm rel}$) is found above the maximum of the ΔH_n. This can happen only because different quantum chemical methods were used to calculate the two curves.

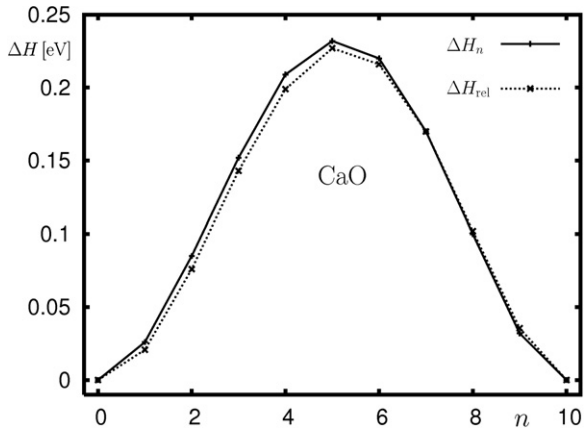

Figure 5. Shown are the same enthalpies as in figure 4 for the B1–B2 transition of CaO. The reference data for $\Delta H_{\rm rel}$ are from Catti's paper [17].

We will show below that MRAM does not give exactly the optimum, but a very good approximation to the optimum path, which has the advantage of much less computational effort.

It can be seen from figure 4 that the enthalpy of activation $\Delta H^{\neq}$ found using MRAM is lower than the maximum of the $\Delta H_{\rm rel}$-curve [25], although $\Delta H_{\rm rel}$ was calculated for an optimized transition path. Even the best estimate, however, cannot be better than the optimum. The reference data ($\Delta H_{\rm rel}$) were obtained from an all electron calculation using atomic basis sets, whereas effective core potentials and a plane wave basis were used for the MRAM values (ΔH_n). Since two different methods were used, $\Delta H^{\neq}$ for the optimized path may indeed be above the value for another path (MRAM).

The good agreement between ΔH_n and $\Delta H_{\rm rel}$ thus only shows that the values obtained from MRAM are physically

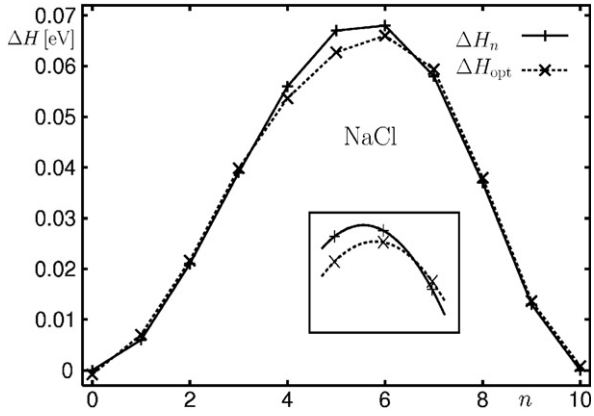

Figure 6. The enthalpy profiles of the B1–B2 transition of NaCl calculated with the same method (LDA, plane wave basis set, Hartwigsen, Goedecker, Hutter pseudopotentials) for the MRAM path (ΔH_n) and for the optimized transition path ($\Delta H_{\rm opt}$). The enthalpy of activation $\Delta H^{\neq}$ obtained for the optimized path is slightly lower than for the MRAM path. In the small picture, the three points around the maximum are shown for both enthalpy curves together with parabolas drawn through them. The abscissa simply enumerates the points of enthalpy along the transition path. A direct comparison between individual $(n, \Delta H_n)$ and $(n, \Delta H_{\rm opt})$ points is, therefore, only meaningful for the initial state ($n = 0$), the final state ($n = 10$), and the transition state (lying at different fractional values of n for the two paths). Minor deviations at ($n = 0$) and ($n = 10$) are due to rounding errors.

meaningful. For a reliable test of MRAM, $\Delta H^{\neq}$ has to be calculated from an optimized transition path with exactly the same method as used for ΔH_n. Consider an alternative formulation of (15).

$$\mathbf{C}_n = a_{\rm B1} c^n \tilde{\mathbf{C}}_n \qquad \tilde{\mathbf{C}}_n = \mathbf{B}\bar{\mathbf{R}}^{10-n}. \tag{16}$$

The shape of the unit cell and the relative position of the ions in it is uniquely given by $\tilde{\mathbf{C}}_n$ for every MRAM structure (16). The sequence of the $\tilde{\mathbf{C}}_n$ ensures that the transition path remains in the subgroup $R\bar{3}m$. Only the volume of the unit cell can be changed without violating this constraint.

It is worth mentioning that the variation of the shape of the unit cell in (16) is given completely by $\tilde{\mathbf{C}}_n$. Thus, a single matrix $\bar{\mathbf{R}}$ is sufficient to describe the B1–B2 transition along the Buerger path for every compound, because the different volumes are contained in the prefactor $a_{\rm B1} c^n$.

For every point along the MRAM path, the energy was calculated for about 10 different volumes by using c^n as a free parameter. These calculations were performed with the same method and the same parameters which were used to compute ΔH_n. In this way, energy curves $E^{(n)}(V)(n = 0, 1, 2, \ldots, 10)$ were obtained. A polynomial of third degree was fitted through every $E^{(n)}(V)$ curve and a volume $\bar{V}^{(n)}$ was determined such that the slope at the point $E^{(n)}(\bar{V}^{(n)})$ corresponds to the precise transition pressure $p_{\rm trans}$. From $E^{(n)}(\bar{V}^{(n)})$ and $\bar{V}^{(n)}$, the enthalpy $\Delta H_{\rm opt}$ was calculated for every n. The values of ΔH_n and of $\Delta H_{\rm opt}$ for NaCl and for CaO are shown in figures 6 and 7, respectively. As expected, for both examples, $\Delta H^{\neq}$ from ΔH_n is found to be slightly higher in enthalpy than the value obtained from the optimized calculation $\Delta H_{\rm opt}$. The

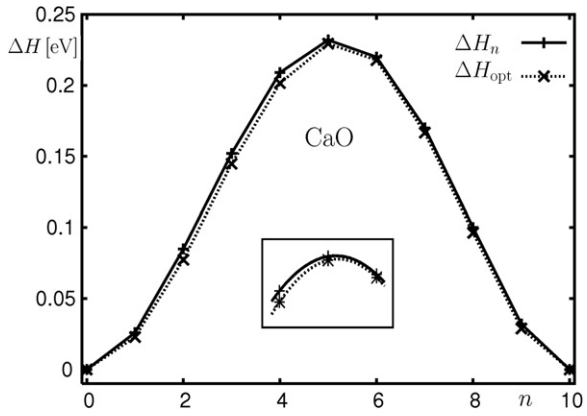

Figure 7. Shown are the same enthalpies as in figure 6 calculated for the B1–B2 transition of CaO.

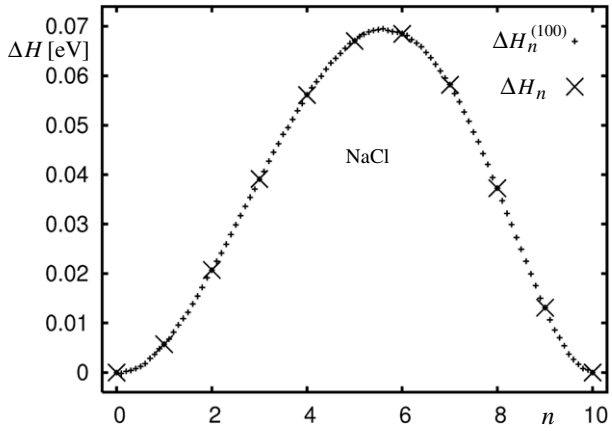

Figure 8. Shown are the same tenth root values ΔH_n from LDA for NaCl as in figure 6 together with $\Delta H_n^{(100)}$-values. They were calculated with the same method for a sequence of structures obtained from the 100th root of **T** instead of its tenth root. Equation (15) had to be adapted in an obvious way. In order to allow for a comparison between both sequences, the step size of the abscissa of the $\Delta H_n^{(100)}$ was set to 1/10. The $\Delta H_n^{(100)}$-values interpolate smoothly between the ΔH_n-values.

computational effort for the calculation of the $\Delta H_{\rm opt}$ was an order of magnitude larger than for the MRAM method.

The MRAM method creates $(n-1)$ reasonable intermediate structures between the initial ($\mathcal{I}$) and the final structure ($\mathcal{F}$). In this way, a good approximation for the transition path is created, as long as the energy landscape between $\mathcal{I}$ and $\mathcal{F}$ is not too complicated. Preliminary calculations indicate that MRAM also works well for a B1–B2 transition within the common subgroup $Pmmn$ [28], whereas it fails for another, more complicated, transition path within the common subgroup $P2_1/m$ [17, 25]. Therefore, MRAM should not be applied as a black box tool to an arbitrary type of transition. The method is, however, very useful if a specific transition type (e.g. the Buerger mechanism) is investigated for a large number of similar compounds across the periodic table, e.g. for all alkaline halides and for all alkaline earth chalcogenides. An expensive test calculation with optimization included is then necessary only for a single test compound in order to check the validity of MRAM for the type of transition under investigation.

Up to this point, all calculations were carried out using the tenth root of **T**. Every other higher root ($n \neq 10$), however, will work as well. As a test, a sequence of intermediate structures between B1 and B2 along the Buerger path was created using the 100th root of **T**. The enthalpies of NaCl calculated with LDA are compared to the corresponding tenth root results in figure 8. The $\Delta H_n^{(100)}$-values look like a smooth interpolation curve between the ΔH_n-points.

For large values of $n = n_{\rm L}$, the path between $\mathcal{I}$ and $\mathcal{F}$ is sampled in very fine intervals. As n decreases, the sampling becomes coarser. The structures created for small values of $n = n_{\rm S} \ll n_{\rm L}$, however, still lie on the transition path given for the limit of very large $n_{\rm L}$, because the, e.g., 17th root or any other $n_{\rm S}$-root can be approximated very accurately by a power of the $n_{\rm L}$th root. An accurate value of the enthalpy of activation from an $n_{\rm S}$ calculation can easily be obtained by parabolic interpolation between the three points of largest enthalpies.

4. Conclusion

In the usual approach, enthalpies between two solid state structures of a compound are calculated along an optimized transition path. This procedure is computationally expensive due to a large number of optimization steps. Our method uses the transition matrix between the two structures and an appropriate nth root of it. It turns out that $n = 10$ is sufficient for a reliable estimation of the transition path. In this way, a new transition path is defined leading to transition enthalpies very similar to those obtained from the usual approach but with much less computational effort. The computer time needed for the calculation of the tenth root is negligible compared to the cost of the quantum chemical calculations.

As can be expected for an interpolation scheme, MRAM is efficient only if the enthalpy landscape along the transition path is not too complicated. Therefore, a test calculation along an optimized path has to be carried out for at least one compound, before MRAM is applied to a new type of transition. If this test has been passed successfully, a whole class of compounds can be treated in a very efficient way.

One might argue that the square root of the transition matrix could be sufficient for the determination of the barrier. For a description of the complete transition path, however, a higher root is necessary. The maximum of the enthalpy along a transition path is not necessarily in the middle between the two structures. Furthermore, for the B1–B2 transition, enthalpy profiles were reported which were not within the subgroup $R\bar{3}m$ and one of which even showed more than one maximum [17, 25].

Acknowledgments

The authors wish to thank Axel Gross, Harold Jones, and Christian Mosch for helpful discussions.

References

[1] Yamamoto T, Iitaka T, Morishita R and Ebisuzaki T 2000 *RIKEN Rev.* **29** 39–41

[2] Vaidya S N and Kennedy G C 1971 *J. Phys. Chem. Solids* **32** 951–64
[3] Mehl M J, Hemley R J and Boyer L L 1986 *Phys. Rev.* B **33** 8685–96
[4] Kalpana G, Palanivel B and Rajagopalan M 1995 *Phys. Rev.* B **52** 4–7
[5] Zimmer H G, Winzen H and Syassen K 1985 *Phys. Rev.* B **32** 4066–70
[6] Huan L, Greene R G and Ruoff A L 1994 *Phys. Rev.* B **49** 15341–3
[7] Schön J C 2004 *Z. Anorg. Allg. Chem.* **630** 2354–66
[8] Sims C E, Barrera G D, Allan N L and Mackrodt W C 1998 *Phys. Rev.* B **57** 11164–72
[9] Uludogan M, Cagin T, Strachan A and Goddard W A III 2001 *J. Comput. Aided Mater. Des.* **8** 192–202
[10] Cervantes P, Williams Q, Côté M, Rohlfing M, Cohen M L and Louie S G 1998 *Phys. Rev.* B **58** 9793–800
[11] Buerger J 1951 *Phase Transformation in Solids* ed R Smoluchowski (New York: Wiley)
[12] Stokes H T and Hatch D M 2002 *Phys. Rev.* B **65** 144114
[13] Zhang S and Chen N–X 2003 *Modelling Simul. Mater. Sci. Eng.* **11** 331–8
[14] Catti M 2004 *J. Phys.: Condens. Matter* **16** 3909–21
[15] Gonze X, Beuken J-M, Caracas R, Detraux F, Fuchs M, Rignanese G-M, Sindic L, Verstraete M, Zerah G, Jollet F, Torrent M, Roy A, Mikami M, Ghosez P, Raty J-Y and Allan D C 2002 *Comput. Mater. Sci.* **25** 478–92
[16] Hartwigsen C, Goedecker S and Hutter J 1998 *Phys. Rev.* B **58** 3641–62
[17] Catti M 2003 *Phys. Rev.* B **68** 100101(R)
[18] Abramowitz M and Stegun I A 1972 *Handbook of Mathematical Functions with Formulas, Graphs, and Mathematical Tables* (*National Bureau of Standards Applied Mathematics Series* vol 55) (Washington, DC: US Govt Printing Office)
[19] Strang G 1986 *Linear Algebra and its Applications* 3rd edn (Fort Worth: Saunders)
[20] Gantmacher F R 1960 *Matrix Theory* vol 1 (New York: Chelsea)
[21] http://www.maplesoft.com/
[22] Murnaghan F D 1944 *Proc. Natl Acad. Sci.* **30** 244–47
[23] Birch F 1947 *Phys. Rev.* **71** 809–24
[24] http://www.gnuplot.info
[25] Catti M 2005 *Symmetry Aspects of Structural Phase Transitions* International School on Mathematical and Theoretical Crystallography Université Henri Poincaré Nancy I www.lcm3b.uhp-nancy.fr/mathcryst/pdf/catti-1.pdf
[26] Perdew J P, Burke K and Ernzerhof M 1996 *Phys. Rev. Lett.* **77** 3865–8
[27] Saunders V R *et al* 1999 *CRYSTAL98: User's Manual* University of Torino Italy, CLRC Daresbury Laboratory, UK
[28] Wanatabe M, Tokonami M and Morimoto N 1977 *Acta Crystallogr.* A **33** 294–8